Research Article Vol. 1, No. 4 / October 2014 / Optica 250

Optical magnetic mirrors without metals

Sheng Liu,[1,2,*] Michael B. Sinclair,[1] Thomas S. Mahony,[1,2] Young Chul Jun,[1,2,3] Salvatore Campione,[1,2,4] James Ginn,[1] Daniel A. Bender,[1] Joel R. Wendt,[1] Jon F. Ihlefeld,[1] Paul G. Clem,[1] Jeremy B. Wright,[1] and Igal Brener[1,2,5]

[1]Sandia National Laboratories, Albuquerque, New Mexico 87185, USA

[2]Center for Integrated Nanotechnologies, Sandia National Laboratories, Albuquerque, New Mexico 87185, USA

[3]Current address: Department of Physics, Inha University, Incheon 402-751, South Korea

[4]Department of Electrical Engineering and Computer Science, University of California Irvine, Irvine, California 92697, USA

[5]e-mail: ibrener@sandia.gov

*Corresponding author: snliu@sandia.gov

Received 30 June 2014; revised 14 August 2014; accepted 14 August 2014 (Doc. ID 214974); published 16 October 2014

The reflection of an optical wave from metal, arising from strong interactions between the optical electric field and the free carriers of the metal, is accompanied by a phase reversal of the reflected electric field. A far less common route to achieving high reflectivity exploits strong interactions between the material and the optical magnetic field to produce a "magnetic mirror" that does not reverse the phase of the reflected electric field. At optical frequencies, the magnetic properties required for strong interaction can be achieved only by using artificially tailored materials. Here, we experimentally demonstrate, for the first time to the best of our knowledge, the magnetic mirror behavior of a low-loss all-dielectric metasurface at infrared optical frequencies through direct measurements of the phase and amplitude of the reflected optical wave. The enhanced absorption and emission of transverse-electric dipoles placed close to magnetic mirrors can lead to exciting new advances in sensors, photodetectors, and light sources.

OCIS codes: (160.3918) Metamaterials; (300.6340) Spectroscopy, infrared; (300.6500) Spectroscopy, time-resolved; (320.7150) Ultrafast spectroscopy; (290.4020) Mie theory.

http://dx.doi.org/10.1364/OPTICA.1.000250

1. INTRODUCTION

Magnetic mirrors or high impedance surfaces were first proposed at microwave frequencies [1]. An important advantage of these mirrors is that a transverse-electric dipole placed close to the mirror surface is located at an antinode of the total (incident plus reflected) electric field and, hence, can absorb and emit efficiently [2]. In contrast, a dipole placed close to a metal surface experiences a node of the total electric field and can neither absorb nor emit efficiently. At microwave frequencies, these exceptional properties of magnetic mirrors have been utilized for smaller, more efficient antennas and circuits [3–6].

At optical frequencies, magnetic behavior can be achieved only through the use of artificially tailored materials and, as a result, relatively little work on optical frequency magnetic mirrors has been reported thus far. Recent investigations of magnetic mirror behavior at optical frequencies have utilized metallic building blocks such as fish-scale structures [7] and gold-capped carbon nanotubes [8]. However, the metals utilized in these approaches suffer from high intrinsic ohmic losses at optical frequencies. All-dielectric metamaterials, based upon subwavelength resonators, with much lower optical losses and isotropic optical response, have been used to demonstrate fascinating properties in a number of recent investigations [9–23]. In another recent work, magnetic mirror behavior was theoretically predicted for silicon dielectric resonators in the near infrared [24]. Although the reflection amplitude spectrum was measured in this work, no experimental phase measurements were achieved. In principle, this work is the same as our previous work [10] that showed only high reflectivity at the magnetic dipole resonance, which is a necessary

but not sufficient condition for magnetic mirror behavior. Moreover, the use of silicon as a resonator material does not result in a sufficiently small array spacing for effective medium behavior, particularly at oblique angles, as discussed in [10]. The benefit of using higher refractive index materials [tellurium (Te) in our work] is clear by comparing the reflectivity amplitude spectra of the silicon structure of [24] and the Te structure in this work: the Te resonators exhibit a much better spectral separation of the electric and magnetic dipole resonances. Recently, theoretical work [25,26] has also predicted nearly total omnidirectional reflection based upon the interplay among different resonant modes of high refractive index resonators. This is in strong contrast to the magnetic mirror behavior obtained in the effective medium limit, which does not depend on the coupling between different resonant modes. Therefore, we present here the first experimental demonstration of an optical magnetic mirror (OMM) using an all-dielectric metamaterial. Furthermore, none of these previous OMM demonstrations, including works that utilized metallic structures, were able to provide detailed temporal information about the optical fields, such as the resonant build-up of the response after transient excitation. In the present work, we overcome these limitations by using an OMM based on a subwavelength two-dimensional array of dielectric resonators fabricated from a low-loss high-permittivity dielectric material: Te. Furthermore, we utilize a phase-sensitive time-resolved optical technique to provide direct experimental proof of the magnetic mirror behavior. We also show that the electric-field standing-wave pattern for plane-wave illumination exhibits an antinode at the surface of the OMM, indicating that efficient coupling to transverse-electric dipoles placed close to the mirror surface should be possible.

2. RESULTS

A. Optical Magnetic Mirror Samples

Figure 1(a) shows a schematic of our magnetic mirror, which comprises a two-dimensional array of subwavelength Te cube resonators. The lowest frequency resonance of a high-permittivity cubic resonator exhibits a circular displacement current pattern, which yields magnetic dipole behavior [10,27], while the next higher resonance leads to a linear displacement current and, hence, electric dipole behavior. The large permittivity of Te [10,27,28] ensures that the dimensions of the resonator and array spacing are sufficiently subwavelength. Two-dimensional arrays of Te resonators were fabricated by depositing Te on a BaF_2 substrate, followed by e-beam lithography patterning and reactive ion etching. The resulting cube-like resonators exhibited a height of 1.7 μm and a base of ~1.5 μm × 1.5 μm (a slight overetching led to the deviation from perfect cube geometry). BaF_2 was selected as a substrate material due to its low reflective index (~1.4) and low loss throughout the IR spectral region. The large refractive index contrast between Te and BaF_2 allows for a high degree of confinement within the Te resonator and small leakage into the substrate [15]. The unit-cell spacing of the array was 3.4 μm for a ~45% duty cycle [10]. Figure 1(b) shows a scanning electron microscope (SEM) image of the fabricated OMM sample. Figure 1(c) shows the measured reflection spectrum of the sample (dotted black curve), which exhibits two reflection maxima that are close to the magnetic and electric dipole resonances [the electric-field patterns are shown as insets in Fig. 1(c)]. The wavelengths of the magnetic (8.95 μm) and electric (7.08 μm) dipole resonances do not precisely correspond to the transmission minima [29], but rather are determined by the loss maxima (i.e., absorption maxima) (see Section S1 of Supplement 1). This selection is also supported by numerical simulations, which show that the strongest dipole field intensities occur close to the wavelengths of maximum absorption (see Section S1 of Supplement 1).

B. Time-Domain Spectroscopy System

To directly measure both the amplitude and phase of the electric field of an optical wave reflected from the OMM, we utilize phase-locked time-domain spectroscopy (TDS) [30]. TDS has proven to be a powerful technique at terahertz frequencies [31–34] and has been recently extended to higher mid-infrared (mid-IR) frequencies [35,36]—a highly interesting frequency region covering vibrational and electronic resonances of molecular systems and solids [37,38]. Figure 2 shows

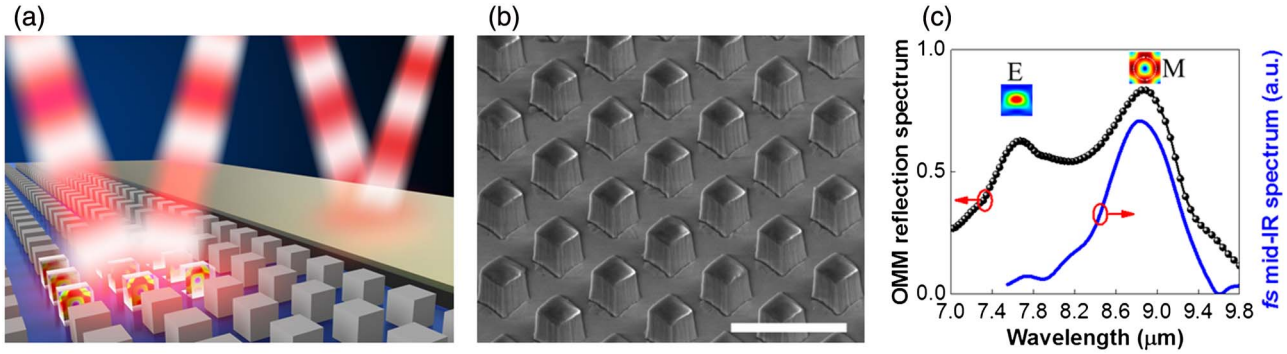

Fig. 1. Principle of all-dielectric OMMs. (a) The cubic dielectric resonators on the left side do not induce a phase shift of the reflected electric field at the magnetic resonance, but rather act as a dielectric magnetic mirror in the optical frequency range. In contrast, the gold surface on the right side (which serves as a reference surface) exhibits a 180 deg phase shift of the electric field upon reflection. (b) SEM image of the Te cube dielectric metasurface of our OMM. The scale bar corresponds to 5 μm. (c) The reflection spectrum (black-dotted curve) of the metamaterial sample in (b) shows two reflection maxima corresponding to the lowest (magnetic dipole) and the second lowest (electric dipole) resonances. The solid blue curve shows the spectrum of the femtosecond mid-IR pulses obtained by performing a Fourier transform of the measured electric field transients as discussed in Section 2.B.

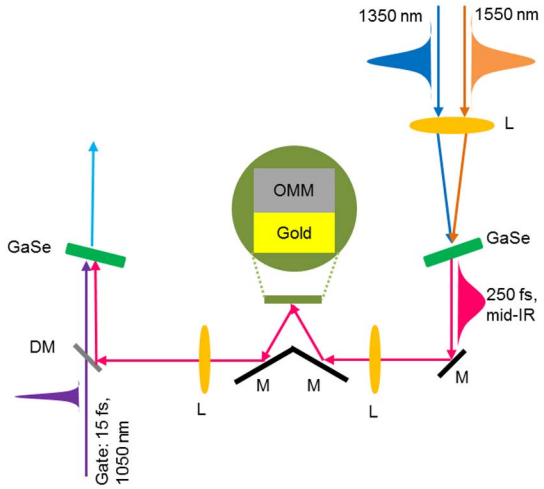

Fig. 2. Schematic of the TDS setup. We used a phase-locked TDS in the mid-IR to directly measure the phase shift of the reflected electric field from the OMM. Mid-IR pulses of 250 fs duration, produced by difference frequency mixing between ~1.35 and ~1.55 μm pulses, were focused by a ZnSe lens onto the OMM or gold surface. Another ZnSe lens was used to collect the reflected mid-IR beam. Gate pulses with a wavelength of 1.05 μm and duration of 15 fs were combined with the mid-IR pulses, using a dichroic mirror, and then focused into another GaSe crystal for phase-matched electro-optic sampling. DM, dichroic mirror; L, lens; M, mirror.

a simplified schematic of our stable-carrier-envelope-phase (CEP)-locked mid-IR TDS system. Briefly, an ultrafast fiber laser system was used to generate ~250 fs mid-IR pulses, tunable between 8.1 and 11 μm. The *p*-polarized pulses were focused onto either the OMM sample or a gold reference surface (which was deposited on top of the Te in an unpatterned region of the sample) at an incidence angle of 30 deg with ~10 deg of angular divergence in the focused beam. Thus, the incident radiation covered a range of angles from 25–35 deg. Care was taken to ensure that switching between the gold and OMM surfaces did not cause any spurious delay change (see Section S2 of Supplement 1). A synchronized 15 fs gate pulse output from the same fiber laser was used to measure the reflected infrared electric-field transients through phase-matched electro-optic sampling in a GaSe crystal [30,39]. The blue curve in Fig. 1(c) shows the spectrum of the femtosecond mid-IR pulses centered at ~8.9 μm obtained by performing a Fourier transform of the electric field transients acquired using the mid-IR TDS technique. More details of our TDS system can be found in Section S3 of Supplement 1, and in [17,40].

C. Phase of the Optical Electric Field Reflected from the Optical Magnetic Mirror

Figure 3(a) shows the measured electric field of the reflected pulses from the OMM (red line) and gold surface (blue line) when the central frequency of the incident pulse coincides with the magnetic dipole resonance of the Te resonators at 8.95 μm. For comparison, Fig. 3(b) is the simulated reflected electric field obtained using a commercial finite-difference time-domain (FDTD) simulator (FDTD Solutions by Lumerical Solutions Inc.), showing remarkable agreement between the

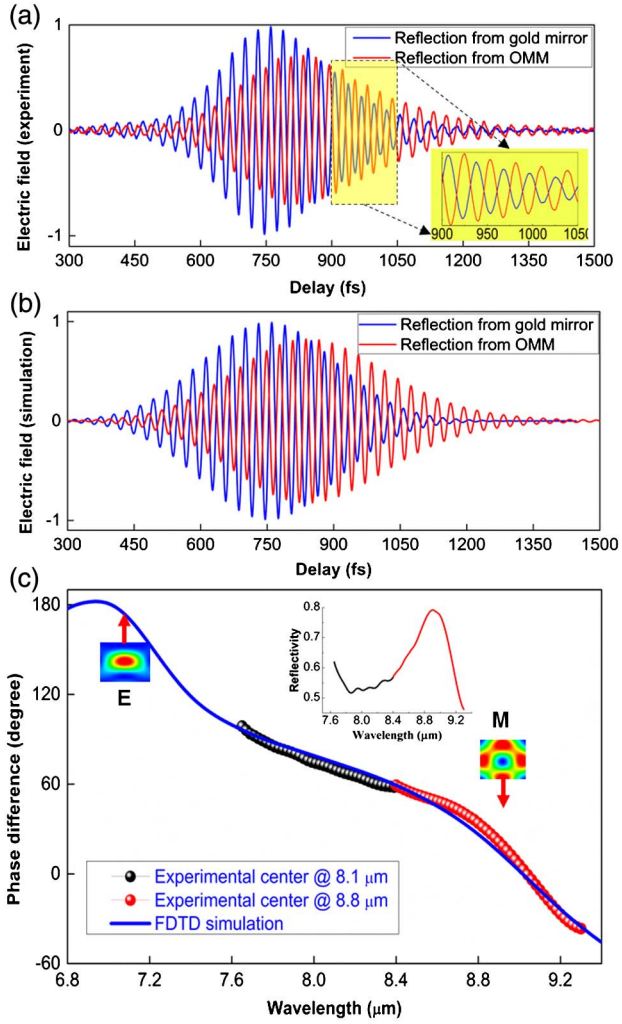

Fig. 3. Electric-field transients measured by TDS. (a) Experimental measurement of the electric field reflected from the gold surface (blue curve) and OMM (red curve) at the OMM magnetic resonance. The gold surface serves as a reference. (b) FDTD simulation of the reflected electric field from the gold surface (blue curve) and the OMM (red curve). Both experiment and simulation show that the electric-field fringes from the OMM are out-of-phase with those from the gold surface (i.e., a normal mirror). This unambiguously demonstrates the magnetic mirror behavior of the OMM. (c) Experimental and FDTD simulation results of the optical phase of the reflected wave. To cover a broader spectral range, two experimental data sets were obtained with the central frequency tuned to 8.8 and 8.1 μm. The inset is the reflectivity of the OMM derived from the Fourier transform of measured field transients.

experimental and simulation data. For both experiment and simulation, the phase of the reflection from the gold surface was referenced to a plane very close to the center of the cubic resonators, which is the plane that contains the radiating dipoles (see Section S4 of Supplement 1). Several features are noticeable in both the measured and simulated waveforms in Figs. 3(a) and 3(b). First, the amplitude of the red curve is slightly smaller than that of the blue curve, indicating that the reflectivity of the OMM is slightly smaller than that of the gold surface (which is close to a perfect mirror in the mid-IR). Second, the reflected field envelope from the OMM has a ~50 fs delay (approximately two optical periods) compared

to that from the gold surface due to the resonant interaction of the optical pulses with the metasurface resonators. Third, and most importantly, the electric-field fringes from the OMM are nearly phase-reversed with respect to the fringes from the gold reference (which are phase-reversed with respect to the incident field). Thus, the electric-field waveforms of Fig. 3(a) demonstrate that the field reflected from the OMM is in-phase with the incident field, which, combined with the high reflection amplitude, directly demonstrates magnetic mirror behavior at wavelengths around 9 μm. Due to the limited wavelength tuning range of the IR pulses, we further studied the phase shift at the electric dipole resonance using FDTD simulations only (see Section S5 of Supplement 1). These simulations show that the electric-field fringes from the OMM are in-phase with those from the gold surface at the electric dipole resonance, because the OMM acts as a normal mirror at this electric resonance frequency.

For a quantitative analysis of the phase difference between the electric fields reflected from gold and the OMM, we performed a Fourier transform of the measured field transients [Fig. 3(c)]. The time harmonic convention $\exp(-i\omega t)$ is implicitly assumed throughout the manuscript. To cover a broader spectral range, a second data set was obtained with the center frequency of the incident mid-IR pulses tuned to ~8.1 μm. The electric-field phase obtained from the FDTD simulation results is also plotted in Fig. 3(c) (blue curve) for comparison. Although the experimental data (red and blue circles) does not reach the electric dipole resonance frequency, it agrees very well with simulations over a wide wavelength region between 7.6 and 9.3 μm. We observe a ~180 deg phase difference between the magnetic and electric dipole resonances, further confirming the magnetic mirror behavior near 9 μm. The inset shows the reflectivity of the OMM calculated by the Fourier transform of the measured field transients. It agrees well with the spectra measured by Fourier transform infrared spectroscopy, exhibiting high reflectivity at the magnetic resonance around 8.9 μm. In addition, we measured another OMM sample made with a different fabrication technique, resulting in a smaller spectral separation between the electric and magnetic dipole resonances. For this sample, our mid-IR pulses are spectrally broad enough to cover both resonances at once (see Section S6 of Supplement 1). Once again, we observe an approximately ~180 deg phase difference between the two dipole resonances, which further demonstrates the OMM behavior at the magnetic dipole resonance. The fact that the behavior does not sensitively depend upon the separation of the electric dipole and magnetic dipole demonstrates that the magnetic mirror behavior does not rely on the coupling between these resonances. We would also like to stress that, due to the symmetric shape of our Te resonators [27], simulation results (not included here) show that the phase behavior is also insensitive to the incoming polarization up to an incidence angle of 45 deg.

To analyze the magnetic mirror behavior, we model each cubic resonator as an electric dipole and a magnetic dipole (whose polarizabilities are calculated via full-wave simulations) located at the center of the cube. We compute the amplitude and phase of the reflection coefficient of the two-dimensional array, including cross coupling between the electric and magnetic dipoles (see Section S4 of Supplement 1) using two-dimensional periodic dyadic Green's functions [41–43] and obtain very good agreement with full-wave simulations. Near the magnetic resonance, the magnetic dipole behavior dominates the optical response and magnetic mirror behavior is observed. In contrast, near the electric resonance, the electric dipole dominates and the array behaves like an electric mirror with an electric field phase shift of 180 deg upon reflection.

D. Emission Enhancement in the Optical Magnetic Mirror Near Field

When a transverse-electric dipole is placed in the near field of a conventional electric mirror, its emission is largely canceled by that of its image dipole [2,44–47]. In contrast, the image dipole produced by a magnetic mirror is in-phase with the original dipole and emission is allowed. Similarly, a transverse-electric dipole in very close proximity to an electric mirror finds itself at the node of the total electric field under plane-wave illumination and cannot efficiently absorb incoming radiation, whereas an electric dipole placed near a magnetic mirror is located at the antinode of the total electric field and can absorb efficiently. As a result, OMM behavior has been studied extensively at microwave frequencies for efficient, compact microwave circuits and antennas [3–6]. To demonstrate that these advantages can also be obtained at optical frequencies, we utilized FDTD simulations to generate maps of the total electric field at both the electric and magnetic resonance wavelengths of the OMM and compared them to the total field maps obtained for a conventional gold mirror. Figure 4(a) shows the standing-wave patterns obtained at the electric resonance wavelength of the OMM for both the OMM and a gold surface. As discussed previously, the gold surface is located at a height equivalent to the center of the dielectric resonators. At the electric resonance, the two standing-wave patterns show similar behavior, with an electric-field node located at the surface of both mirrors. The behavior is distinctly different at the OMM magnetic resonance wavelength [Fig. 4(b)], where an electric-field antinode is observed at the surface of the OMM. As expected, the gold mirror still exhibits a surface node at this wavelength. (Media 1 shows plane waves reflected from a gold surface and an OMM which are in-phase and out-of-phase at the electric and magnetic resonances, respectively.) Closer inspection of Fig. 4(b) shows that the total electric field exhibits some enhancement at the mirror surface, which is presumably due to the resonant nature of the OMM. Hence, at this wavelength, dipole absorbers/emitters placed in the immediate vicinity of the OMM surface are expected to interact strongly with the total field and efficiently absorb/emit electromagnetic energy. Indeed, we observe a large enhancement of dipole radiative emission when a transverse-electric dipole at the magnetic resonance wavelength is placed close to the OMM, as shown in Fig. 5. Using full wave simulation tools, the radiative decay rate is calculated by measuring the outgoing flux from a dipole source and normalizing it by the flux in free space. We calculate the normalized radiative decay rate of a transverse electric dipole oscillating at the magnetic resonance frequency as a function of the dipole–surface separation for

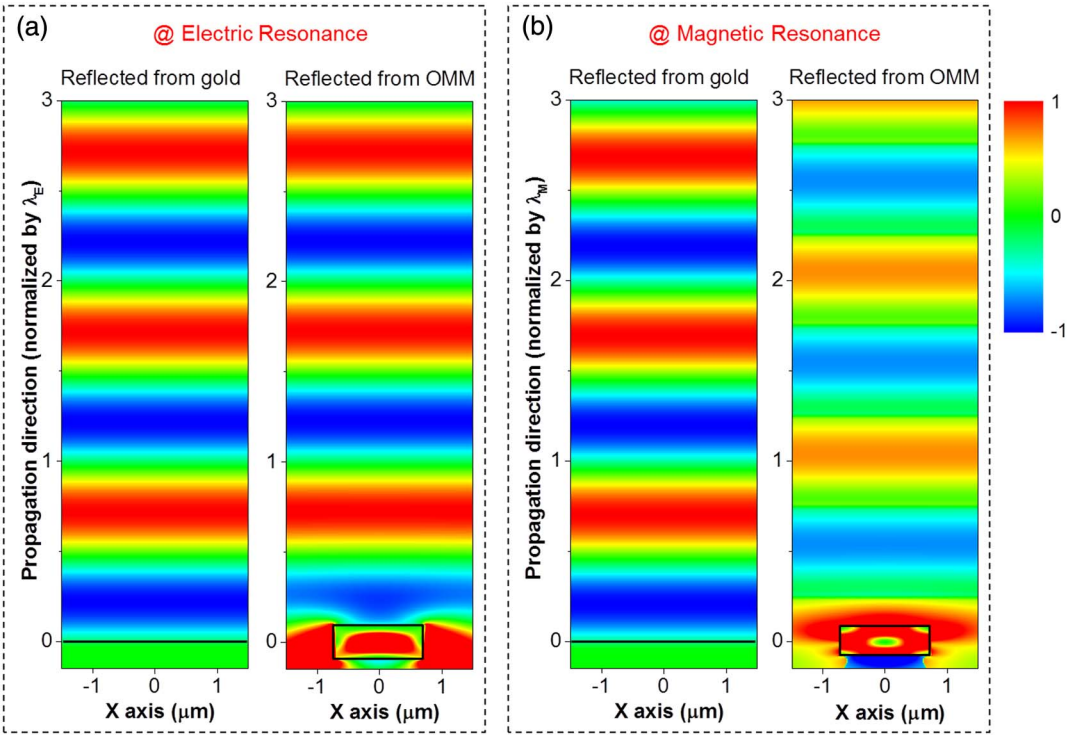

Fig. 4. Standing-wave patterns of light reflected from a gold mirror and an OMM at (a) the OMM electric resonance and (b) the OMM magnetic resonance. The OMM behaves like a conventional mirror at the electric resonance shown in (a) and behaves like a magnetic mirror at the magnetic resonance shown in (b) Media 1. The black lines and rectangles represent the gold–air interfaces and the boundaries of the Te cubic resonators, respectively. A node of the standing wave always occurs at the gold–air interface. In contrast, the top of the cubic resonator is at the node for the electric resonance and at the antinode for the magnetic resonance. All patterns share the same color scale bar on the right. Also note that the aspect ratio used for this figure causes the profile of the cubic resonator to appear as a rectangle.

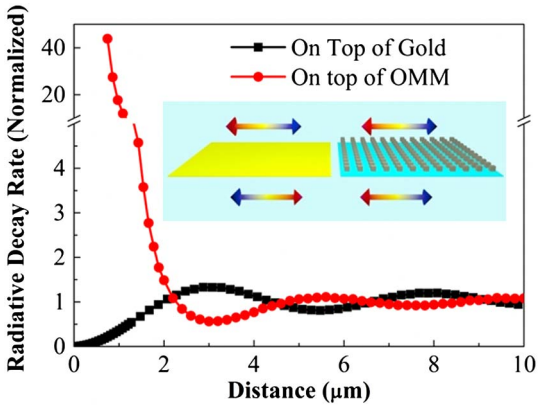

Fig. 5. Normalized radiative decay rate of a transverse-electric dipole oscillating at the magnetic resonance frequency as a function of the dipole–surface separation for both a 5 × 5 array approximating our OMM (red curve) and a gold surface (black curve). The distance of the dipole from the OMM is calculated using the center of the cubic resonator as distance "0," which is in agreement with our theoretical calculation (Section 4 of Supplement 1). First, the oscillatory dependence on distance is shifted by about half a period. Second, while the emission from the dipole is quenched very close to the gold surface, the dipole emission near the magnetic mirror is enhanced even for very small distances. Inset: a schematic of an electric dipole placed on top of a typical mirror and its reversed image dipole (left) and a schematic of an electric dipole on top of a dielectric magnetic mirror and its unreversed image dipole (right) at the magnetic dipole resonance.

both a 5 × 5 resonator array approximating our OMM and a gold surface. The behavior for these two cases is strikingly different: (i) the oscillatory dependence on distance is shifted by about half a period, which is a further confirmation of the magnetic mirror behavior of the OMM; (ii) while the emission from the dipole is quenched very close to the gold surface, the dipole emission rate near the magnetic mirror is enhanced even for very small distances. We also calculate the ratio of radiative decay rate to total decay rate to be ~53% when the transverse dipole is very close (10 nm) to the top surface of the Te resonators. The nonradiative loss is due to the nonzero imaginary part of the Te permittivity. However, the emission from the transverse dipole in the near field of the OMM is more complicated than what is expected from simple image dipole arguments, possibly due to coupling to higher order modes of the 5 × 5 array.

3. CONCLUSIONS

We experimentally demonstrated the OMM behavior of low-loss all-dielectric metasurfaces through direct measurements of the phase and amplitude of the reflected optical wave. We also showed that all-dielectric magnetic mirrors are good candidates for new types of infrared sensors, such as remotely interrogated chemical sensors in which molecular species adsorbed onto chemically selective layers on the mirror surface will interact strongly with the interrogating radiation and impart spectral

signatures on the reflected beam. In addition, these mirrors will be useful for compact and efficient thermal radiation sources in which thermal emitters are deposited directly on the mirror surface and the emitted thermal energy is efficiently coupled to the far field. Further, we envision that, through appropriate metasurface design, it should be possible to produce an admixture of magnetic mirror and electric mirror behaviors to achieve a pre-desired angular response for the amplitude and phase of reflected waves.

FUNDING INFORMATION

U.S. Department of Energy (DOE) (DE-AC04-94AL85000).

ACKNOWLEDGMENTS

This work was performed, in part, at the Center for Integrated Nanotechnologies, a U.S. Department of Energy, Office of Basic Energy Sciences user facility. Portions of this work were supported by the Laboratory Directed Research and Development program at Sandia National Laboratories. Sandia National Laboratories is a multi-program laboratory managed and operated by Sandia Corporation, a wholly owned subsidiary of Lockheed Martin Corporation, for the U.S. Department of Energy's National Nuclear Security Administration under contract DE-AC04-94AL85000. We thank Larry K. Warne for useful technical discussions.

See Supplement 1 for supporting content.

REFERENCES

1. D. Sievenpiper, Z. Lijun, R. F. J. Broas, N. G. Alexopolous, and E. Yablonovitch, "High-impedance electromagnetic surfaces with a forbidden frequency band," IEEE Trans. Microwave Theor. Tech. **47**, 2059–2074 (1999).
2. J. D. Jackson, *Classical Electrodynamics* (Wiley, 1999).
3. A. Erentok, P. L. Luljak, and R. W. Ziolkowski, "Characterization of a volumetric metamaterial realization of an artificial magnetic conductor for antenna applications," IEEE Trans. Antennas Propag. **53**, 160–172 (2005).
4. A. P. Feresidis, G. Goussetis, S. H. Wang, and J. C. Vardaxoglou, "Artificial magnetic conductor surfaces and their application to low-profile high-gain planar antennas," IEEE Trans. Antennas Propag. **53**, 209–215 (2005).
5. D. J. Kern, D. H. Werner, A. Monorchio, L. Lanuzza, and M. J. Wilhelm, "The design synthesis of multiband artificial magnetic conductors using high impedance frequency selective surfaces," IEEE Trans. Antennas Propag. **53**, 8–17 (2005).
6. A. Vallecchi, J. R. De Luis, F. Capolino, and F. De Flaviis, "Low profile fully planar folded dipole antenna on a high impedance surface," IEEE Trans. Antennas Propag. **60**, 51–62 (2012).
7. A. S. Schwanecke, V. A. Fedotov, V. V. Khardikov, S. L. Prosvirnin, Y. Chen, and N. I. Zheludev, "Optical magnetic mirrors," J. Opt. A Pure Appl. Opt. **9**, L1–L2 (2007).
8. H. Rostami, Y. Abdi, and E. Arzi, "Fabrication of optical magnetic mirrors using bent and mushroom-like carbon nanotubes," Carbon **48**, 3659–3666 (2010).
9. I. Staude, A. E. Miroshnichenko, M. Decker, N. T. Fofang, S. Liu, E. Gonzales, J. Dominguez, T. S. Luk, D. N. Neshev, I. Brener, and Y. Kivshar, "Tailoring directional scattering through magnetic and electric resonances in subwavelength silicon nanodisks," ACS Nano **7**, 7824–7832 (2013).
10. J. C. Ginn, I. Brener, D. W. Peters, J. R. Wendt, J. O. Stevens, P. F. Hines, L. I. Basilio, L. K. Warne, J. F. Ihlefeld, P. G. Clem, and M. B. Sinclair, "Realizing optical magnetism from dielectric metamaterials," Phys. Rev. Lett. **108**, 097402 (2012).
11. L. Shi, J. T. Harris, R. Fenollosa, I. Rodriguez, X. Lu, B. A. Korgel, and F. Meseguer, "Monodisperse silicon nanocavities and photonic crystals with magnetic response in the optical region," Nat. Commun. **4**, 1904 (2013).
12. S. Person, M. Jain, Z. Lapin, J. J. Sáenz, G. Wicks, and L. Novotny, "Demonstration of zero optical backscattering from single nanoparticles," Nano Lett. **13**, 1806–1809 (2013).
13. P. Moitra, Y. Yang, Z. Anderson, I. I. Kravchenko, D. P. Briggs, and J. Valentine, "Realization of an all-dielectric zero-index optical metamaterial," Nat. Photonics **7**, 791–795 (2013).
14. Y. H. Fu, A. I. Kuznetsov, A. E. Miroshnichenko, Y. F. Yu, and B. Luk'yanchuk, "Directional visible light scattering by silicon nanoparticles," Nat. Commun. **4**, 1527 (2013).
15. P. Spinelli, M. A. Verschuuren, and A. Polman, "Broadband omnidirectional antireflection coating based on subwavelength surface Mie resonators," Nat. Commun. **3**, 692 (2012).
16. L. Shi, T. U. Tuzer, R. Fenollosa, and F. Meseguer, "A new dielectric metamaterial building block with a strong magnetic response in the sub-1.5-micrometer region: silicon colloid nanocavities," Adv. Mater. **24**, 5934–5938 (2012).
17. M. K. Schmidt, R. Esteban, J. J. Sáenz, I. Suárez-Lacalle, S. Mackowski, and J. Aizpurua, "Dielectric antennas—a suitable platform for controlling magnetic dipolar emission," Opt. Express **20**, 13636–13650 (2012).
18. A. E. Miroshnichenko and Y. S. Kivshar, "Fano resonances in all-dielectric oligomers," Nano Lett. **12**, 6459–6463 (2012).
19. A. I. Kuznetsov, A. E. Miroshnichenko, Y. H. Fu, J. Zhang, and B. Luk'yanchuk, "Magnetic light," Sci. Rep. **2**, 492 (2012).
20. A. E. Krasnok, A. E. Miroshnichenko, P. A. Belov, and Y. S. Kivshar, "All-dielectric optical nanoantennas," Opt. Express **20**, 20599–20604 (2012).
21. J. M. Geffrin, B. García-Cámara, R. Gómez-Medina, P. Albella, L. S. Froufe-Pérez, C. Eyraud, A. Litman, R. Vaillon, F. González, M. Nieto-Vesperinas, J. J. Sáenz, and F. Moreno, "Magnetic and electric coherence in forward- and back-scattered electromagnetic waves by a single dielectric subwavelength sphere," Nat. Commun. **3**, 1171 (2012).
22. A. B. Evlyukhin, S. M. Novikov, U. Zywietz, R. L. Eriksen, C. Reinhardt, S. I. Bozhevolnyi, and B. N. Chichkov, "Demonstration of magnetic dipole resonances of dielectric nanospheres in the visible region," Nano Lett. **12**, 3749–3755 (2012).
23. K. Seo, M. Wober, P. Steinvurzel, E. Schonbrun, Y. Dan, T. Ellenbogen, and K. B. Crozier, "Multicolored vertical silicon nanowires," Nano Lett. **11**, 1851–1856 (2011).
24. J. Z. Hao, Y. Seokho, L. Lan, D. Brocker, D. H. Werner, and T. S. Mayer, "Experimental demonstration of an optical artificial perfect magnetic mirror using dielectric resonators," in *IEEE Antennas and Propagation Society International Symposium* (IEEE, 2012), pp. 1–2.
25. J. Du, Z. Lin, S. T. Chui, G. Dong, and W. Zhang, "Nearly total omnidirectional reflection by a single layer of nanorods," Phys. Rev. Lett. **110**, 163902 (2013).
26. C. J. Chang-Hasnain and W. Yang, "High-contrast gratings for integrated optoelectronics," Adv. Opt. Photon. **4**, 379–440 (2012).
27. S. Liu, J. F. Ihlefeld, J. Dominguez, E. F. Gonzales, J. E. Bower, D. B. Burckel, M. B. Sinclair, and I. Brener, "Realization of tellurium-based all dielectric optical metamaterials using a multi-cycle deposition-etch process," Appl. Phys. Lett. **102**, 161905 (2013).
28. Y. Fink, J. N. Winn, S. Fan, C. Chen, J. Michel, J. D. Joannopoulos, and E. L. Thomas, "A dielectric omnidirectional reflector," Science **282**, 1679–1682 (1998).
29. F. Capolino, A. Vallecchi, and M. Albani, "Equivalent transmission line model with a lumped X-circuit for a metalayer made of pairs of planar conductors," IEEE Trans. Antennas Propag. **61**, 852–861 (2013).
30. S. Liu, T. S. Mahony, D. A. Bender, M. B. Sinclair, and I. Brener, "Mid-infrared time-domain spectroscopy system with carrier-envelope phase stabilization," Appl. Phys. Lett. **103**, 181111 (2013).

31. N. Jukam, S. S. Dhillon, D. Oustinov, J. Madeo, C. Manquest, S. Barbieri, C. Sirtori, S. P. Khanna, E. H. Linfield, A. G. Davies, and J. Tignon, "Terahertz amplifier based on gain switching in a quantum cascade laser," Nat. Photonics **3**, 715–719 (2009).
32. J. Kroll, J. Darmo, S. S. Dhillon, X. Marcadet, M. Calligaro, C. Sirtori, and K. Unterrainer, "Phase-resolved measurements of stimulated emission in a laser," Nature **449**, 698–701 (2007).
33. B. Ferguson and X.-C. Zhang, "Materials for terahertz science and technology," Nat. Mater. **1**, 26–33 (2002).
34. H.-T. Chen, W. J. Padilla, J. M. O. Zide, A. C. Gossard, A. J. Taylor, and R. D. Averitt, "Active terahertz metamaterial devices," Nature **444**, 597–600 (2006).
35. Q. Wu and X. C. Zhang, "Free-space electro-optics sampling of mid-infrared pulses," Appl. Phys. Lett. **71**, 1285–1286 (1997).
36. R. Huber, A. Brodschelm, F. Tauser, and A. Leitenstorfer, "Generation and field-resolved detection of femtosecond electromagnetic pulses tunable up to 41 THz," Appl. Phys. Lett. **76**, 3191–3193 (2000).
37. R. Huber, F. Tauser, A. Brodschelm, M. Bichler, G. Abstreiter, and A. Leitenstorfer, "How many-particle interactions develop after ultrafast excitation of an electron-hole plasma," Nature **414**, 286–289 (2001).
38. G. Gunter, A. A. Anappara, J. Hees, A. Sell, G. Biasiol, L. Sorba, S. De Liberato, C. Ciuti, A. Tredicucci, A. Leitenstorfer, and R. Huber, "Sub-cycle switch-on of ultrastrong light-matter interaction," Nature **458**, 178–181 (2009).
39. A. Sell, A. Leitenstorfer, and R. Huber, "Phase-locked generation and field-resolved detection of widely tunable terahertz pulses with amplitudes exceeding 100 MV/cm," Opt. Lett. **33**, 2767–2769 (2008).
40. A. Benz, S. Campione, S. Liu, I. Montaño, J. F. Klem, A. Allerman, J. R. Wendt, M. B. Sinclair, F. Capolino, and I. Brener, "Strong coupling in the sub-wavelength limit using metamaterial nanocavities," Nat. Commun. **4**, 2882 (2013).
41. S. Steshenko, F. Capolino, P. Alitalo, and S. Tretyakov, "Effective model and investigation of the near-field enhancement and subwavelength imaging properties of multilayer arrays of plasmonic nanospheres," Phys. Rev. E **84**, 016607 (2011).
42. S. Campione, F. Mesa, and F. Capolino, "Magnetoinductive waves and complex modes in two-dimensional periodic arrays of split ring resonators," IEEE Trans. Antennas Propag. **61**, 3554–3563 (2013).
43. S. Campione, M. B. Sinclair, and F. Capolino, "Effective medium representation and complex modes in 3D periodic metamaterials made of cubic resonators with large permittivity at mid-infrared frequencies," Photon. Nanostr. Fundam. Appl. **11**, 423–435 (2013).
44. C. A. Balanis, *Antenna Theory: Analysis and Design* (Wiley, 2005).
45. E. Yablonovitch, "Inhibited spontaneous emission in solid-state physics and electronics," Phys. Rev. Lett. **58**, 2059–2062 (1987).
46. K. H. Drexhage, "Influence of a dielectric interface on fluorescence decay time," J. Lumin. **1–2**, 693–701 (1970).
47. W. L. Barnes, "Fluorescence near interfaces: the role of photonic mode density," J. Mod. Opt. **45**, 661–699 (1998).